THE JOURNAL OF BIOLOGICAL CHEMISTRY
Vol. 275, No. 28, Issue of July 14, pp. 21514–21524, 2000

Printed in U.S.A.

Structural and Functional Studies with Antibodies to the Integrin β2 Subunit

A MODEL FOR THE I-LIKE DOMAIN*

Received for publication, March 17, 2000
Published, JBC Papers in Press, April 21, 2000, DOI 10.1074/jbc.M002286200

Chichi Huang‡, Qun Zang§, Junichi Takagi¶, and Timothy A. Springer¶‖

From the ¶Center for Blood Research and Department of Pathology, Harvard Medical School, Boston, Massachusetts 02115, ‡Pfizer Central Research, Groton, Connecticut 06340, and §Biogen, Cambridge, Massachusetts 02142

To establish a structure and function map of the β2 integrin subunit, we mapped the epitopes of a panel of β2 monoclonal antibodies including function-blocking, nonblocking, and activating antibodies using human/mouse β2 subunit chimeras. Activating antibodies recognize the C-terminal half of the cysteine-rich region, residues 522–612. Antibodies that do not affect ligand binding map to residues 1–98 and residues 344–521. Monoclonal antibodies to epitopes within a predicted I-like domain (residues 104–341) strongly inhibit LFA-1-dependent adhesion. These function-blocking monoclonal antibodies were mapped to specific residues with human → mouse knockout or mouse → human knock-in mutations. Combinatorial epitopes involving residues distant in the sequence provide support for a specific alignment between the β-subunit and I domains that was used to construct a three-dimensional model. Antigenic residues 133, 332, and 339 are on the first and last predicted α-helices of the I-like domain, which are adjacent on its "front." Other antigenic residues in β2 and in other integrin β subunits are present on the front. No antigenic residues are present on the "back" of the domain, which is predicted to be in an interface with other domains, such as the α subunit β-propeller domain. Most mutations in the β2 subunit in leukocyte adhesion deficiency are predicted to be buried in the β2 subunit I-like domain. Two long insertions are present relative to α-subunit I-domains. One is tied down to the back of the I-like domain by a disulfide bond. The other corresponds to the "specificity-determining loop" defined in β1 and β3 integrins and contains the antigenic residue Glu^{175} in a disulfide-bonded loop located near the "top" of the domain.

Integrins are αβ heterodimers that bind both cell surface and extracellular matrix ligands (1). The leukocyte or β2 integrins act as traffic signal molecules to regulate leukocyte emigration from the bloodstream in inflammation and lymphocyte homing (2). Additionally, the leukocyte integrin LFA-1 (CD11a/CD18) is important in lymphocyte/antigen-presenting cell and killer cell/target cell interactions in immune responses (3). LFA-1 binds to the immunoglobulin superfamily members intercellular adhesion molecules 1, 2, and 3 (ICAM-1, -2, and -3).[1] Mutations in the β2 integrin subunit cause leukocyte adhesion deficiency (LAD), a disease characterized by life-threatening bacterial infections, granulocytosis, and a lack of neutrophil diapedesis at inflammatory sites (4).

Ligand binding by integrins is dynamically regulated by cellular signals (5, 6). The adhesiveness of β2 integrins can be transiently stimulated after cellular activation through receptor tyrosine kinases and G protein-coupled receptors and can be stably activated with phorbol esters, Mn^{2+}, or activating mAb. The mechanisms of activation of β2 integrins appear to include both conformational changes that regulate the affinity or multivalent affinity (avidity) for ligand and association with the cytoskeleton.

Regions in the N-terminal segments of integrin α and β subunits are important for ligand binding. All integrin α subunits contain seven repeats of ~60 residues each that are predicted to fold into a β-propeller domain containing seven β-sheets (7). The β-propeller is toroidal in shape, with the β-sheets arranged around a central pseudosymmetry axis like blades of a propeller. Some integrins, including the leukocyte integrins, contain a functionally important inserted (I) domain between β-propeller sheets 2 and 3. The I domain has a doubly twisted fold that is found in nucleotide-binding enzymes and G proteins, with a central hydrophobic β-sheet surrounded by amphipathic α-helices (8–11). Five residues in a central pocket coordinate with Mg^{2+} either directly or via water molecules to form a metal ion-dependent adhesion site (MIDAS). During ligand binding, the sixth coordination position of the Mg^{2+} is hypothesized to be occupied by an acidic residue in the ligand (8). This residue in ICAM-1 is likely to correspond to Glu-34, which is by far the most critical residue for binding to LFA-1 (12). Mutation in I domains of the residues that form the primary or secondary coordination shell of the Mg^{2+} abolishes ligand binding (reviewed in Ref. 8). Specificity for ICAM-1 maps to amino acid residues on either side of the Mg^{2+} (13). Furthermore, mAbs that map to the I domain, but not mAbs that map to surrounding regions in the β-propeller domain, block ligand binding by LFA-1 (13). These results show that the I domain in the α subunit of LFA-1 constitutes a ligand binding interface for ICAM-1.

The domain structure for integrin β subunits is less well defined than for α subunits. A region that is highly conserved among integrin β subunits is located between residues 104 and 341 of the β2 subunit. This region is 94% identical between mouse and human β2, and amino acid substitutions that cause

* This work was supported by National Institutes of Health Grant CA 31798. The costs of publication of this article were defrayed in part by the payment of page charges. This article must therefore be hereby marked "*advertisement*" in accordance with 18 U.S.C. Section 1734 solely to indicate this fact.

‖ To whom correspondence should be addressed: Dept. of Pathology, Center for Blood Research and Harvard Medical School, 200 Longwood Ave., Boston, MA 02115. Tel.: 617-628-5343; Fax: 617-278-3232; E-mail: springer@sprsgi.med.harvard.edu.

[1] The abbreviations used are: ICAM, intercellular adhesion molecule; mAb, monoclonal antibody; LAD, leukocyte adhesion deficiency; MIDAS, metal ion-dependent adhesion site; PCR, polymerase chain reaction; vWF, von Willebrand's factor; PMA, phorbol 12-myristate 13-acetate.

TABLE I
Nucleotide sequences used for constructing the human/mouse chimeras or point mutants

Mutants	Overlap sequences[a]	Restriction site[b]
h98m	CCCTTGGCCCTCCGGAA	*Bsp*EI
h163m	AAGGAGAAAGCTTGCCAGCCCCC	*Hin*dIII
m254h	CTGGGCGCCATCCTGACCCCC	
h301m, m302h	GCGGTGACAAAGAAGATGGTGAA	No *Bst*EII site
h344m, m344h, HmH	ATAAACTCTCCTCACGCGTCTTCCTGG	*Mlu*I
R122N	GACCTCAACAATGTCAAGAAGCTTGGTGG	*Hin*dIII
R133Q	GGTGGAGATCTGCTCCAGGCCCTC	*Bgl*II
D163E	CACCCTGAGAAGCTTCGAAACCC	*Hin*dIII
E175A	AAGGAGAAAGCTTGCCAGCCCCC	*Hin*dIII
N190D	GTGCTGAAGCTTACCGACAACTCC	*Hin*dIII
M218I	CGCCATCATGCAGGTCGCCGCATGCCCGG	*Sph*I
L270M	GACAACATGTACAAGAGATCTAACGAATTCGAC	*Bgl*II
A290S/N292S	GCGCACAAGCTTTCTGAAAGCAACATC	*Hin*dIII
S302K/R303K	GCGGTGACAAAGAAGATGGTGAA	No *Bst*EII site
E325D	CTGTCTGATGACTCGAGCAATGTG	*Xho*I
H332Q	GAGGACTCGAGCAATGTGGTCCAACTCATT	*Xho*I

Mutants	PCR primer[c]	Restriction site[b]
m122h	CCACCAAGCTTCTTGACATTGTTGAGGTC	*Hin*dIII
m163h	GGGTTTCGAAGCTTCTCAGGGTG	*Hin*dIII
h254m	AAGCTGGGCGCCATCCTGACCCCC	
m521h	TGGCTGTTATAGCGCTCACAGTTGAC	
h612h	GAGTGCCTGAAGTTCGAAAAGGGCCCC	*Bst*BI
m612h	GGGGCCCTTTTCGAACTTCAGGCACTC	*Bst*BI
N339Y, R133Q/N339Y, R133Q/H332Q/N339Y	AGGAAGACGCGTGAGGAGAGTTTATAGTATGCATTC	*Nsi*I

[a] The complementary overlap sequences of primers for overlap extension PCR. Restriction sites introduced by silent mutation are underlined.
[b] Restriction sites were introduced or deleted for screening the mutants.
[c] 5′ end primers (h254m, h612m, L132A, R133A, L135A) or 3′ end primers (m122h, m163h, m521h, m612h, N339Y) were used to construct chimeras or point mutants. All sequences are shown 5′ to 3′.

LAD map to this region (reviewed in Ref. 14). Ligand cross-linking, mutational, and mAb mapping studies suggest that this conserved region is functionally important (15, 16). Blocking and stimulatory mAb have been mapped to this region in β1 and β3 integrins (16, 17). A MIDAS-like D*X*S*X*S motif is present in the conserved region, and the conserved region has been proposed to have an I domain-like fold (8, 18, 19). Mutation of the Asp and two Ser residues of the D*X*S*X*S motif as well as other residues in the conserved region with oxygenated side chains abolishes ligand binding in several β integrins. Alignment of hydropathy plots shows good similarity between the first half of the α subunit I domain and the β subunit conserved region (8); however, the second half diverges, suggesting that there are important structural differences in this region. The end of the putative I-like domain is therefore difficult to define. The only previously published three-dimensional model of an I-like domain, for that of the β3 subunit (18), proposed that it terminated at the equivalent of residue 284 in β2. A different structure-sequence alignment has been proposed that places the domain terminus at residue 341 (19); however, no specific three-dimensional model was proposed.

Cysteine-rich regions are present N-terminal and C-terminal to the β-subunit I-like domain and are linked by a long range disulfide bond. The N-terminal cysteine-rich region is homologous to a repeat found in plexins, semaphorins, and integrins (PSI domain) (20). mAbs that activate integrins have been mapped to the C-terminal cysteine-rich region in β1 and β3 integrins (21–26), and the KIM127 mAb has been mapped to residues 413–575 in β2, in the middle third of the region C-terminal to the I-like domain (27). Epitopes for several other activating mAbs defined for β2 integrins, CBR LFA-1/2 (28) and KIM185 (29), have not been well localized. While there is no evidence that it participates in ligand binding, the C-terminal region may be important in transducing signals from inside the cell that regulate ligand binding.

To explore the structure and function of the β2 subunit, we have mapped epitopes of a panel of 17 mouse anti-human β2 mAbs and one rat anti-mouse β2 mAb, including function-blocking, nonblocking, and activating mAbs. Nonblocking mAbs map outside the I-like domain, and activating mAbs map to the C-terminal region. The function-blocking antibodies map to the I-like domain, and we have been able to define individual human/mouse amino acid substitutions responsible for five different antibody epitopes in this region. Several epitopes involve residues that are distant in the primary structure and provide constraints on the folding of this region that are used to predict its structure, in conjunction with secondary structure and threading prediction algorithms, sequence-structure alignments, and molecular modeling.

MATERIALS AND METHODS

Cell Lines and Monoclonal Antibodies—COS-7, JY, and SKW3 cells were grown in RPMI 1640 medium supplemented with 10% fetal bovine serum. The mouse anti-human CD18 IgG1 monoclonal antibodies TS1/18 (30), CBR LFA-1/1, CBR LFA-1/2, CBR LFA-1/7 (28), and anti-human CD11a mAb TS1/22 (30) were previously described. Antibody 1C11 was obtained through the Fourth International Leukocyte Workshop. Antibodies 6.7 (31), CLB LFA-1/1 (32), and L130 were obtained through the Fifth International Leukocyte Workshop. mAb MHM23 (33) was a gift from Dr. A. McMichael. CLB-54 (34) was a gift from Dr. R. Van Lier. GRF1 (35) was a gift from Dr. F. Garrido. MEM-48 (36) was a gift from Dr. V. Horejsí. 11H6 was a gift from Dr. H. J. Bühring. May.017 (37) was a gift of Dr. Y. Ohashi. KIM185 (29) and 6.5e were gifts of Dr. M. Robinson. Rat anti-human antibodies YFC51.1 and YFC118.3 (38) were gifts from Dr. G. Hale. Addresses for the above antibody contributors are listed in Refs. 39 and 40. The rat anti-mouse CD18 mAb C71/16 (41) was from Dr. I. Trowbridge (Salk Institute, San Diego, CA).

Human and Mouse Chimeric CD18 Constructs—Both human and murine β2 cDNA were in Ap^{r}M8 (13). Chimeras were named according to the species origin of their segments. For example, h98m indicates that residues 1–98 are from the human β subunit and residues 99 to the C terminus are from the mouse β subunit. Amino acid sequence numbering was according to the mature human sequence (42). The primers used for generating chimeras and substitution mutants are listed in Table I. In most of the cases, silent mutations were introduced into the primers to create a restriction site for testing of incorporation of the mutations. Polymerase chain reaction (PCR) was used to construct

chimeras h612m, m612h, m521h, m122h, m163h, and h254m. To construct h612m, a DNA fragment from residue 612 to the C terminus of murine β2 subunit (mβ2) was generated by PCR, digested with *Bst*BI and *Not*I, and ligated to a 7.7-kilobase pair DNA fragment generated from human β2 (hβ2) with the same enzymes. Chimeras m612h and m521h were constructed by insertion of PCR fragments (*Hin*dIII-612 or *Hin*dIII-521) amplified from mβ2 into *Hin*dIII and *Bst*BI or *Hin*dIII and *Eco*47III sites of hβ2. The *Hin*dIII site is located on the 5′ end of the cloning site of the vector Ap^{r}M8. Constructs m122h and m163h were made by insertion of the PCR fragments (*Hin*dIII-122 or *Hin*dIII-163) from mβ2 into *Hin*dIII sites created in the human to mouse mutants R122N or D163E. h254m was made by ligation of a PCR fragment (*Kas*I–*Mlu*I) from mβ2 into the *Kas*I and *Mlu*I sites of h344m.

Other chimeras were constructed by PCR overlap extension (43). In brief, two successive PCRs were used to generate a chimeric fragment, which was then digested with restriction enzymes and ligated into the hβ2, mβ2, or certain chimeric constructs. In the first PCR, two separate PCRs were used to generate one fragment from hβ2 and a neighboring fragment from mβ2. Two oligonucleotide primers at the overlap region were complementary for at least 24 bases. A silent substitution in the sequence of the overlap oligonucleotide was included to introduce a restriction site for screening of clones and for construction of subsequent chimeras. Chimeras h344m and m344h were constructed by inserting chimeric PCR fragments into *Hin*dIII and *Bst*BI sites on h612m or hβ2, respectively. A silent mutation was included to introduce a *Mlu*I site on residue 344. The constructs, h302m, h163m, and h98m, or m302h and m254h, were made by insertion of the chimeric PCR fragments into restriction sites *Hin*dIII and *Mlu*I in h344m or m344h, respectively.

Construction of Human → Mouse Point Mutations—To facilitate the construction of point mutants in the conserved region, a silent mutation was introduced into hβ2 to create a unique *Mlu*I restriction site at residue 344 by PCR overlap extension as described above. The PCR fragment containing the *Mlu*I site was ligated into the *Hin*dIII and *Bst*BI sites of hβ2. The mutant, HmH, was verified by sequencing and expression on the COS cell surface and binding to ICAM-1 (not shown). The mutant N339Y was generated by PCR amplification with primers that overlapped the *Bsu*36I and *Mlu*I sites and encoded mutations near the *Mlu*I site. The PCR fragment was then transferred into the *Bsu*36I and *Mlu*I sites of HmH. PCR overlap extension was used to produce the other point mutants. To create mutants L270M, A290S/N292S, S302K/R303K, E325D, and H332Q, 5′ upstream and 3′ downstream primers containing the *Bsu*36I and *Mlu*I sites, respectively, were used to generate PCR fragments that were then ligated into the HmH. Similarly, mutants R122N, R133Q, D163E, E175A, N190D, and M218I were generated by using primers encompassing the *Hin*dIII and *Kas*I sites. The PCR fragments were digested with these enzymes and ligated into hβ2. The double point mutants R133Q/H332Q and R133Q/N339Y were constructed by replacing the *Hin*dIII–*Kas*I fragment of H332Q or N339Y with the *Hin*dIII–*Kas*I fragment of R133Q. The triple point mutant R133Q/H332Q/N339Y was made by PCR amplification with R133Q/H332Q as template and primers that contained the *Bsu*36I and *Mlu*I site and that encoded the N339Y mutation near the *Mlu*I site. All point mutants were verified by sequencing about 100 base pairs around the mutation sites.

Construction of Mouse → Human Point Mutations—Individual human residues were introduced into the murine β subunit sequence by PCR overlap extension (43). Briefly, the outer 5′ and 3′ primers were selected to include unique restriction sites near the mutation in the β subunit cDNA. Mutations were introduced by a pair of inner complementary primers. After PCR, the products were restriction-digested and ligated into the β subunit cDNA vector cut with the same enzymes. All constructs were verified by DNA sequencing of the region subjected to PCR.

Aggregation Assay—JY or SKW3 cells used for aggregation assays were harvested near confluence (about 5×10^5 cells/ml). After 20 min of preincubation with ascites (1:200) or purified mAbs (10 μg/ml), cells were stimulated with phorbol 12-myristate 13-acetate (PMA) at a final concentration of 50 ng/ml in 100 μl of L-15 medium (Sigma) supplemented with 5% fetal bovine serum. The reactions were performed in microtiter plates gently shaken for 30 min for JY cells or 2 h for SKW cells at 37 °C. The amount of aggregation was scored as described (13).

Cell Transfection and Immunofluorescence Flow Cytometry—cDNAs in Ap^{r}M8 expression vector were purified by Wizard Midiprep kits (Promega, Madison, WI) and ethanol-precipitated. COS cells were transiently co-transfected with wild-type, mutant, or chimeric β2 subunits and human αL subunit cDNA constructs using DEAE-dextran (44). Transfected COS cells were treated with trypsin-EDTA on day 2 and replated. On day 3, cells were harvested in 5 mM EDTA/phosphate-buffered saline and washed with L-15 medium supplemented with 2.5% fetal bovine serum.

Results with human → mouse mutations were repeated, and mouse → human knock-in mutations were tested, using transfection of 293T cells with calcium phosphate precipitates (45, 46). Medium was changed after 7–11 h. Cells were harvested for flow cytometry analysis 48 h after transfection.

Immunofluorescence flow cytometry was performed as described (47). Cells were incubated with 10 μg/ml purified mAb or a 1:200 dilution of ascites on ice for 30 min and then stained with a 1:20 dilution of fluorescein isothiocyanate-conjugated secondary antibody. After washing, the cells were resuspended and fixed in PBS containing 1% formaldehyde.

Adhesion Assay—Transfected COS cells were labeled with 2′,7′-bis-(2-carboxyethyl)-5-(and -6)-carboxyfluorescein acetoxymethyl ester (Molecular Probes, Inc., Eugene, OR) and assayed for binding to ICAM-1 as described (13). Binding of mutant transfected cells to ICAM-1 was expressed as a percentage of wild-type transfectant binding, *i.e.* 100 × (mutant − mock binding)/(wild-type − mock binding). Triplicates in each experiment were averaged and considered as a single data point for calculation of S.D. among at least three different experiments.

Secondary Structure Predictions—Thirty-six integrin β subunits from six different phyla, Swiss-Prot or GenBank™ accession codes P05107, P11835, S32659, P32592, P53714, P53713, P055563, P09055, P49134, P07228, P12606, P26010, P26011, S43534, O54890, P05106, I51530, P18084, AF043257, P18564, U77584, AF078802, AF059607, A57283, P11584, AF060203, X98852, AF005356, P26012, P26013, P16144, JN0786, Q64632, AF005357, and L13305 were aligned with PRRP with human β2 as the top sequence (48). The I-like domain and 10 adjoining residues on either end were excised. All columns with gaps in the human β2 sequence were removed from the alignment, and it was submitted as an SAF file to PHD (49).

Threading—Threading was with THREADER V2.1a (50) (available on the World Wide Web). The data base of 1908 representative chains and files was updated as described previously (51). To this was added the 351 domains and chains with a three-layer αβα sandwich architecture, *i.e.* each homology family representative from the CATH Database H-level Representatives List with the 3.40 architecture (52) (available on the World Wide Web). Domains were cut out of pdb files using the CATH domain definition list. Additionally, one representative for each conformationally distinct integrin I-domain and von Willebrand's factor A domain structure was added. Domains and chains were converted to THREADER data base format using STRSUM. A total of 2321 structures were present in the data base.

Sequence segments corresponding to residues 102–341 of integrin β2 from all 35 integrin β subunits described above were subjected to threading. Because of the insertions expected in the β subunit I-like domain compared with currently known structures, different loop gap penalty weights were tested (0.5, 0.45, 0.4, 0.35, and 0.30). The energies (pairwise plus solvation) for each structure were averaged for the 35 sequences, and *Z*-scores for the average energies were calculated with the histogram tool of Excel. Weights of 0.45–0.35 grouped I and A domains together in terms of their scores and thus gave the most consistent results, although the highest *Z*-score for any structure was obtained with the weight of 0.5 (4.72 with the αM I domain).

Molecular Modeling—The I domain structures of integrin αM, 1jlm (9); αL, 1zon (53); α2, 1aox (11); and the A1 and A3 domains of vWF, respectively, 1auq (54) and 1atz (55), were superimposed with 3DMALIGN of MODELLER (56) (available on the World Wide Web), using a gap penalty of 4 Å and five iterations of alignment with superposition of Cα, Cβ, Cα, Cβ, and finally Cα atoms. The superimposed structures and the resulting structure-sequence PIR alignment were opened in LOOK (Molecular Applications Group, Palo Alto, CA), and multiple gaps within each loop were condensed into a single gap, leaving insertions/deletions near turns or midpoints of loops. The β2 sequence was aligned using both secondary structure and sequence similarity, as described under "Results." In early models, the specificity-determining loop (57) of β2 was omitted. A LOOK model with 1atz as template was used as the .ini file in MODELLER, to obtain better starting positions for untemplated loops. All five I and A domain structures were used as templates in MODELLER with the alignment of Fig. 4, and an extra β-ribbon in the Cheb methylesterase structure 1chd, residues 233–248, was used as a template for β2 residues 253–268. Because the 1chd template did not overlap any of the other templates, its position relative to the rest of the domain was only restrained by the disulfide between Cys^{224} and Cys^{264}. Of 100 models, that with the best score with the QUACHK module of WHATIF (58) was chosen. Both this model and the I domain structures

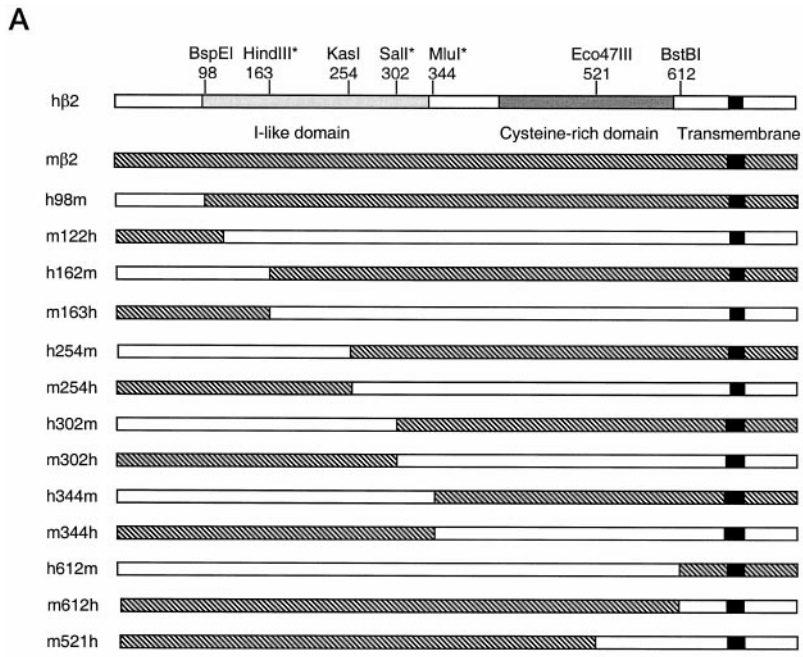

B

Antibody	h	m	h98m	m122h	h162m	m163h	h254m	m254h	h302m	m302h	h344m	m344h	m521h	h612m	m612h	Epitope
TS1/22	+	+	+	+	+	+	+	+	+	+	+	+	+	+	+	hCD11a
C71/16	-	+	-	+	-	+	-	+	-	+	-	+	+	-	+	1-98
11H6	+	-	-	-		-	+	-	+	-	+	-	-	+	-	99-122
GRF1	+	-	-	+	+	-	+	-	+	-	+	-	-	+	-	123-162
TS1/18	+	-	-	+	+	+	+	+	+	+	+	-	-	+	-	123-163/303-344
YFC51.1	+	-	-	+	-	-	-	-	-	-	+	-	-	+	-	123-163/303-344
YFC118.3	+	-	-	+	-	-	-	-	-	-	+	-	-	+	-	123-163/303-344
1C11	+	-	-	+	+	+	+	+	+	+	+	-	-	+	-	123-163/303-344
CLB LFA1/1	+	-	-	+	-	+	-	+	-	+	+	-	-	+	-	303-344
CLB-54	+	-	-	+	-	+	-	+	-	+	+	-	-	+	-	303-344
L130	+	-	-	+	-	+	+	-	+	-	+	-	-	+	-	164-254
MHM23	+	-	-	+	-	+	+	-	+	-	+	-	-	+	-	164-254
6.5e	+	-	-	+	-	+	+	-	+	-	+	-	-	+	-	164-254
MAY.017	+	-	-	+	+	+	+	-	+	-	+	-	-	+	-	123-162/164-254
CBR LFA-1/7	+	-	-	+		+	-	+	-	+	-	+	-	+	-	345-612
6.7	+	-	-	+		+	-	+	-	+	-	+	-	+	-	345-612
MEM48	+	-	-	+		+	-	+	-	+	-	+	-	+	-	345-612
CBR LFA-1/2	+	-	-	+		+	-	+	-	+	-	+	+	+	-	522-612
KIM185	+	-	-	+		+	-	+	-	+	-	+	+	+	-	522-612

FIG. 1. **Structure of chimeric β2 integrin subunits and mAb epitope localization.** *A*, the human β2 subunit (hβ2) is shown with domains and restriction sites; sites with *asterisks* were introduced with silent mutations to facilitate the construction of chimeras. *Numbers* correspond to amino acid residues in the mature human β2 sequence (42). In chimeras, *open* and *hatched bars* correspond to human and mouse sequence, respectively. *B*, mapping of epitopes on the β2 subunit. mAb reactivity was determined by immunofluorescent flow cytometry on COS cells cotransfected with the indicated wild-type or chimeric β2 subunits and the human αL subunit. Scoring was as follows: +, percentage of positive cells comparable with the wild-type transfectant; −, staining not significantly different from the negative control (mock transfectant).

were used as templates in a further round of modeling in which the specificity-determining loop, β2 residues 149–176, was inserted. For the loop bonded by the Cys^{169}–Cys^{176} disulfide, a disulfide-bonded loop of the same length was used, residues 5–13 of the CD59 complement-regulating protein structure 1cdq. 400 models were made, and one without knotted loops and with good QUACHK and NQACHK scores was chosen.

RESULTS

Mapping of Epitopes on the β2 Integrin Subunit—13 human/mouse β subunit chimeras were constructed to map mAb epitopes and correlate localization in the structure with the effect of mAb on function (Fig. 1*A*). Proper association with the α subunit was shown by immunofluorescence staining with αL mAb of COS cells cotransfected with the chimeric β and the human αL subunits. Expression of αL on the cell surface requires association with the β2 subunit (47, 59). All 13 chimeric β2 subunits associated with the human αL subunit and were expressed on the cell surface as efficiently as wild-type human and murine β2 subunits as shown with TS 1/22 mAb to αL (Fig. 1*B*). Furthermore, the function of all 13 chimeric β2 subunits associated with αL in transfected COS cells was demonstrated by binding to purified human ICAM-1 and was equivalent to human αLβ2 (data not shown).

The chimeras were used to map the epitopes of a panel of 17 mouse mAbs to the human β2 subunit and one rat mAb to the mouse β2 subunit using immunofluorescence flow cytometry of transfected COS cells (Fig. 1*B*). The rat mAb to mouse CD18, C71/16, bound to an epitope contained within residues 1–122, as shown with m122h, and at least a portion of the epitope localized N-terminal to residue 98, as shown with h98m. This mAb thus maps N-terminal to the conserved domain.

Three mAbs, 6.7, MEM-48, and CBR LFA-1/7, were shown with reciprocal chimeras to bind to an epitope localized between residue 345 and 612, and the absence of staining of m521h further showed that the epitope included amino acids between residues 345 and 521. These mAbs thus map C-terminal to the conserved domain.

Two of the antibodies studied, CBR LFA-1/2 and KIM185, activate binding of β2 integrins to their ligands (28, 29). These mAbs mapped to the C-terminal half of the cysteine-rich region, from residue 522 to 612.

Further mAb mapped to discrete regions within the conserved region (Fig. 1*B*). The epitope recognized by mAb 11H6 included residues 99–122. The mAb GRF1 bound to an epitope between residues 123 and 163, as shown with chimeras h163m,

m163h, h254m, and m254h. mAbs L130, MHM23, and 6.5e bound to the region between residues 164 and 254. mAb May.017 bound to both chimeras m163h and h163m. Lack of reactivity with h98m and m254h showed that this mAb recognizes residues in at least two segments, from 98 to 163 and from 164 to 254. mAb CLB LFA-1/1 and CLB 54 mapped to residues 303–344.

Two pairs of antibodies exhibited complex patterns of reactivity, suggesting recognition of epitopes in noncontiguous conserved subregions. mAbs YFC51.1 and YFC118.3 bound to an epitope between residues 122 and 344, as shown with chimeras m122h, h344m, and m344h. However, these mAbs failed to stain three pairs of reciprocal chimeras, h163m and m163h, h254m and m254h, and h302m and m302h. Thus, replacement of either the N-terminal portion (residues 122–163) or C-terminal portion (residues 302–344) of the conserved domain destroyed the epitope. This suggested that mAb YFC51.1 and YFC118.3 recognize an epitope requiring the presence of amino acid residues from both regions 123–163 and 302–344.

The staining pattern of mAbs TS1/18 and 1C11 was converse to that of mAb YFC51.1 and YFC118.3. These two mAbs could also be localized to an epitope between residues 123 and 344. However, mAb TS1/18 and 1C11 bound to all three pairs of the reciprocal chimeras h163m and m163h, h254m and m254h, and h302m and m302h. Even when these mAbs were titered and used at concentrations just sufficient to give good staining of hβ2, no significant difference in staining intensity between these reciprocal chimeras and hβ2 was detected (not shown). The binding to all three reciprocal chimeras suggests that recognition of one of two regions, which are split in all three chimeras, is sufficient for binding. Thus, the epitope includes residues from both regions 123–163 and 303–344, and the presence of human residues from either of these regions is sufficient for binding.

Mapping Epitopes to Individual Residues in the I-like Domain—Only 14 amino acid residues in the I-like domain differ between the mouse and human, simplifying mapping of epitopes to specific amino acid residues. Site-directed mutagenesis was used to introduce individual mouse amino acid residues into the human β2 integrin sequence (Fig. 2A). Residues found to be important were further studied by introducing mouse → human substitutions into the mouse β2 subunit, co-expression with the human αL subunit, and testing for gain of mAb reactivity (Fig. 2*B*). The mAb mapping results are described in light of a model for the I-like domain, which is described below (Figs. 4 and 5).

mAb CLB LFA-1/1 and CLB 54 map to the predicted C-terminal α-helix of the I-like domain. In agreement with mapping of these mAbs to residues 303–344, the human → mouse substitutions H332Q and N339Y reduced binding partially and completely, respectively (Fig. 2*A*). Expression of a mouse β2 subunit containing three mouse → human substitutions (Q133R, Q332H, and Y339N) yielded gain of expression of the CLB LFA-1/1 and CLB 54 epitopes, whereas the double mouse → human mutant Q133R/Q332H was negative (Fig. 2*B*). Together, the knock-out and knock-in data demonstrate that both His^{332} and Asn^{339} contribute to this epitope. These residues are seven sequence positions apart in the predicted C-terminal α-helix of the β2 subunit, the α6-helix (see below; Fig. 4). Since an α-helix makes one turn per 3.5 residues, these residues are exactly two turns away from one another, on the same face of the predicted α-helix, as appropriate for their presence in the same epitope (see below; Fig. 5).

Five mAb (GRF1, YFC51.1, YFC118.3, TS1/18, and 1C11) map to both the first and last predicted α-helices of the I-like domain. For GRF1, the knock-out R133Q mutation demonstrated the importance of Arg^{133} (Fig. 2*A*). The knock-in Q133R mutation confirmed the importance of Arg^{133}, but the knock-in mutation Q332H also demonstrated a role for His^{332} (Fig. 2*B*). Furthermore, the double knock-in Q133R/Q332H bound the GRF1 mAb better than either single mutation, confirming the presence of both Arg^{133} and His^{332} in the epitope (Fig. 2*B*). The TS1/18 mAb was unaffected by knock-out of any single human residue, but binding was abolished by the double mutation R133Q/H332Q (Fig. 2*A*). Binding of TS1/18 was partially restored by knock-in of either Arg^{133} or His^{332} and completely restored by knock-in of both residues in the Q133R/Q332H mutant (Fig. 2*B*). The binding of YFC51.1 and YFC118.1 mAb was abolished by both the R133Q mutation and by the H332Q mutation (Fig. 2*A*). In agreement, single knock-ins of either Arg^{133} or His^{332} had no effect, but knocking the double Q133R/Q332H mutation into the mouse β-subunit completely reconstituted binding of YFC51.1 and YFC118.1 (Fig. 2*B*). Binding of the 1C11 mAb was not affected by the single R133Q or N339Y mutations but was eliminated by the double mutant R133Q/N339Y. Introduction of Arg^{133} into the murine sequence was not sufficient to restore binding, nor was the double knock-in Q133R/Q332H; however, the triple knock-in Q133R/Q332H/Y339N reconstituted binding. Thus, Arg^{133} and Tyr^{339} are important in the 1C11 epitope.

The epitope mapping of the above five mAbs is in excellent agreement with the model described below, which shows that residues Arg^{133}, His^{332}, and Asn^{339} are in adjacent α-helices (see below; Fig. 5). Indeed, these residues form a triangle, and each pair of residues that forms a side of the triangle is recognized by a different set of antibodies: Arg^{133} and His^{332} by GRF1, TS1/18, YFC51.1, and YFC118.1; Arg^{133} and Asn^{339} by

A Mouse residues substituted into human β2

mAb	h	R122N	R133Q	D163E	E175A	N190D	M218I	L270M	A290S/N292S	R302K/N303S	E325D	H332Q	N339Y	R133Q/H332Q	R133Q/N339Y	R133Q/H332Q/N339Y	Epitope
TS1/22	+	+	+	+	+	+	+	+	+	+	+	+	+	+	+	+	αL
11H6	+	-	+	+	+	+	+	+	+	+	+	+	+				122+ ?
GRF1	+	+	-	+	+	+	+	+	+	+	+	+	+	-	-	-	133+332
TS1/18	+	+	+	+	+	+	+	+	+	+	+	+	+	-	+	-	133+332
YFC51.1	+	+	-	+	+	+	+	+	+	+	+	-	+	-	-	-	133+332
YFC118.1	+	+	-	+	+	+	+	+	+	+	+	-	+	-	-	-	133+332
1C11	+	+	+	+	+	+	+	+	+	+	+	+	+	+	-	-	133+339
CLB LFA-1/1	+	+	+	+	+	+	+	+	+	+	+	+/-	-	+/-	-	-	332+339
CLB 54	+	+	+	+	+	+	+	+	+	+	+	+/-	-				332+339
L130	+	+	+	+	-	+	+	+	+	+	+	+	+				175
MHM23	+	+	+	+	-	+	+	+	+	+	+	+	+				175
6.5e	+	+	+	+	-	+	+	+	+	+	+	+	+				175
May.017	+	+	+	+	+	+	+	+	+	+	+	+	+				175+ ?

B Human residues substituted into mouse β2

mAb	h	m	N122R	A175E	N122R/A175E	Q133R	Q332H	Q133R/Q332H	Q133R/Q332H/Y339N	Epitope
TS1/22	+	+	+	+	+	+	+	+	+	αL
11H6	+	-	-	-	-	-	-	-	-	122+ ?
GRF1	+	-	-	-	-	+/-	+/-	+	+	133+332
YFC51.1	+	-	-	-	-	-	-	+	+	133+332
YFC118.1	+	-	-	-	-	-	-	+	+	133+332
TS1/18	+	-	-	-	-	+/-	+/-	+	+	133+332
1C11	+	-	-	-	-	+	-	+	+	133+339
CLB LFA-1/1	+	-	-	-	-	-	-	-	+	332+339
CLB 54	+	-	-	-	-	-	-	-	+	332+339
L130	+	-	-	+	+	-	-	-	-	175
MHM23	+	-	-	+	+	-	-	-	-	175
6.5e	+	-	-	+	+	-	-	-	-	175
May.017	+	-	-	+	+	-	-	-	-	175+ ?

FIG. 2. **Localization of epitopes with individual amino acid substitutions.** *A*, introduction of mouse residues into human β2 (knock-out). *B*, introduction of human residues into mouse β2 (knock-in). mAb reactivity was determined by immunofluorescent flow cytometry on COS cells and in independent experiments on 293T cells. Cells were cotransfected with the indicated mutant β subunits and the human αL subunit or vector control. Scoring was as follows. +, percentage of positive cells comparable with the wild-type transfectant; ±, percentage of positive cells markedly less than wild-type transfectant but significantly higher than the negative control; −, staining not significantly different from the mock transfectant negative control (mock).

TABLE II
Inhibition of PMA-stimulated SKW3 and JY cell aggregation with mAb to the β2 subunit

mAb	Epitope	Aggregation score[a]		Aggregation[b]	
		SKW3	JY	SKW3	JY
				%	%
X63 control		4+	4+	97 ± 9	94 ± 3
6.7	345 − 521	3+	3+	81 ± 6	73 ± 11
MEM-48	345 − 521	4+	4+	97 ± 3	96 ± 2
CBR LFA-1/7	345 − 521	4+	3+	92 ± 6	93 ± 2
CBR LFA-1/2	522 − 612	4+	4+	95 ± 12	97 ± 1
May.017	175 + ?	1+	1+	2 ± 2	1 ± 4
TS1/18	133 + 332	1+	1+	2 ± 3	2 ± 1
1C11	133 + 339	1+	1+	3 ± 6	1 ± 1
11H6	122	2+	2+	42 ± 9	26 ± 7
6.5e	175	1+	1+	5 ± 2	7 ± 4
L130	175	2+	2+	12 ± 11	22 ± 18
MHM23	175	1+	1+	3 ± 5	2 ± 1
GRF1	133 + 332	2+	2+	19 ± 11	50 ± 5
YFC51.1	133 + 332	1+	1+	5 ± 2	0 ± 1
YFC118.3	133 + 332	1+	1+	2 ± 5	3 ± 3
CLB-54	332 + 339	1+	1+	3 ± 5	4 ± 2
CLB LFA1/1	332 + 339	1+	1+	6 ± 4	2 ± 1

[a] Aggregation was scored as described (74), where 1+ indicates less than 10% of the cells were in aggregates; 2+ indicates that 10–50% of the cells were in aggregates; 3+ indicates that 50–100% of the cells were in small loose clusters; 4+ indicates that up to 100% of the cells were in large clusters; and 5+ indicates that all cells were in large, very compact aggregates.

[b] After the aggregation assay, one-tenth of the cells were transferred to a fresh microtiter well, and free cells were counted in four different microscope grids. Aggregation = 100 × (1 − (free cells with mAb)/(free cells without PMA)). Data are mean ± S.D. of three independent experiments. In the absence of PMA, no aggregation occurred.

1C11; and His^{332} and Asn^{339} by CLB LFA-1/1 and CLB 54.

Four antibodies map within a short segment closed by a disulfide between Cys^{169} and Cys^{176}, which has been shown in the β1 and β3 integrin subunits to determine ligand specificity (57). The E175A knock-out mutation abolishes recognition by mAb L130, MHM23, and 6.5e (Fig. 2*A*). The A175E knock-in mutation is sufficient for binding of these three mAbs and additionally May.017 (Fig. 2*B*). The ability of A175E to knock in binding of May.017 and the inability of E175A to knock out binding are consistent with the finding that human residues 1–162 are sufficient for May.017 binding (Fig. 1*B*). Residues 1–98 are not sufficient. All of the human residues in the 99–162 interval have been knocked in individually and do not restore May.017 binding; therefore, it appears possible that two or more residues in the 99–162 interval, or one in this interval and another in the 1–98 interval, contribute to the epitope.

Inhibition of Lymphoid Cell Homotypic Aggregation with mAbs to β2—Two lymphoid cell lines, JY and SKW3, were used to test the ability of CD18 mAbs to block the interactions of LFA-1 with ICAM-1 and ICAM-3. JY cells express ICAM-1, less ICAM-2, and no ICAM-3. On the other hand, SKW3 cells express ICAM-3, less ICAM-2, and no ICAM-1. In agreement with this, the homotypic aggregation of PMA-stimulated JY and SKW3 cells is mediated predominantly by LFA-1 interaction with ICAM-1 and ICAM-3, respectively (60, 61). The inhibition of homotypic aggregation of JY and SKW3 cells by β2 subunit mAbs was concordant (Table II). Furthermore, there was an excellent correlation between the epitopes to which mAb bound and their effect on function. Antibodies that bound C-terminal to the I-like domain were not inhibitory. Of these mAb, those that bound more C-terminally were the ones that have previously been shown to activate LFA-1 adhesiveness: CBR LFA-1/2, KIM185, MEM48 (28, 29), and, according to previous mapping results, KIM127 (27). All 12 mAbs that mapped to the I-like domain were inhibitory (Table II), despite binding to at least five distinct classes of epitopes within this domain.

A Prediction of a Fold for the Conserved Domain—The secondary structure and solvent accessibility of the β2 subunit were predicted by PHD (49), using as input a multiple alignment containing 35 integrin β-subunits (see "Materials and Methods") including all eight β subunits known in *Vertebrata* and subunits from five other phyla: *Arthropoda*, *Echinodermata*, *Nematoda*, *Cnidaria*, and *Porifera*. The predicted secondary structure for the entire extracellular domain is shown to scale (Fig. 3). The PSI-like domain in the first 50 residues of β2 contains two predicted α-helices. The only other predicted α-helices are in the region corresponding to the I-like domain; these α helices alternate with predicted β-strands, as previously noted (19, 62), and thus the I-like domain is predicted to have an α/β fold. Between the PSI domain and the I-like domain are four predicted β-strands. The region C-terminal to the I-like domain contains approximately 20 predicted β-strands. The predicted β-strands in the I-like domain are hydrophobic, as appropriate for a three-layer αβα sandwich containing a central hydrophobic β-sheet and surrounding amphipathic helices. By contrast, the β-strands N- and C-terminal to the I-like domain have alternating hydrophobic and hydrophilic amino acids, as appropriate to two-layer ββ sandwiches. Because of the above considerations, and also the I-like domain's greater conservation in evolution, it is justifiable to segment out the I-like domain as an α/β domain between all-β domains and to consider it separately for structure prediction.

Threading with THREADER 2.1 and an up-dated fold data base was used to identify a fold for the I-like domain. In threading, a sequence is aligned with or "threaded through" each structure in a data base. The sequence-structure alignments are completely analogous to sequence-sequence alignments, including provision for gaps or insertions, but what is calculated is the pseudoenergy of the test sequence in each three-dimensional structure in the data base. The sequence corresponding to residues 102–341 of β2 for each of the 35 different integrin β subunits was threaded, and scores for each structure in the fold data base were averaged for all 35 sequences. Previous results on threading the I-like domain gave inconsistent results for the two different β subunits that were studied, and the fold data base did not include any integrin I or vWF A domains (19). Averaging results for multiple homologous sequences yields more reliable results (51, 63). Six integrin I domain and vWF A domain structures were in the data base, and all six were among the top seven structural hits (Table III). Furthermore, the remaining structure among the top seven hits, 1chd, is a member of the same fold family,

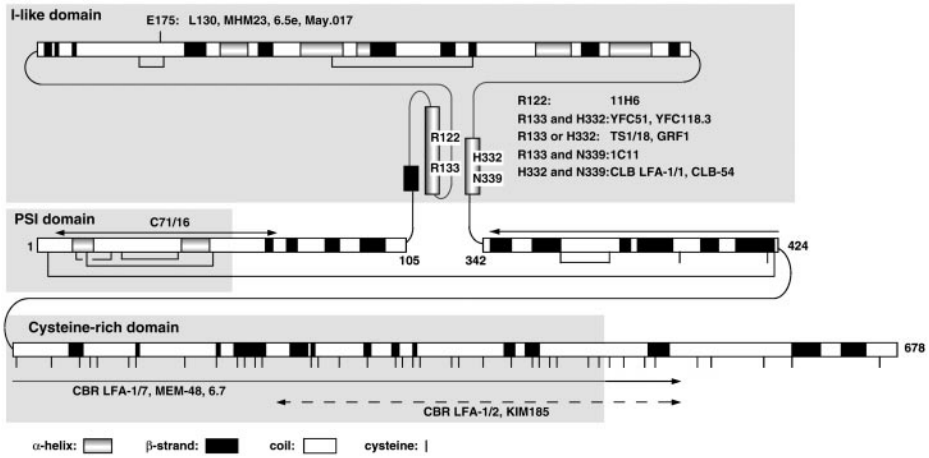

FIG. 3. **Predicted secondary structure, domain organization, and epitope localization of the β2 integrin extracellular segment.** Secondary structure was predicted with PHD using a multiple sequence alignment of 35 integrin β subunits as described under "Materials and Methods." The lengths of predicted secondary structure segments are shown to scale, along with cysteines and confidently defined disulfide bonds in β3 (75).

TABLE III
Averaged threading results for 35 β-subunit I-like domains

Threading was as described under "Materials and Methods" with a gap penalty of 0.45. Energies for each of 2321 structures were averaged for I-like domains from 35 different integrin β-subunits. *Z*-scores were calculated, and the highest scoring structures are shown. According to the Threader 2 User Guide (50), "Experience has shown the following interpretations to be useful: $Z > 3.5$, very significant, probably a correct prediction; $Z > 2.9$, significant, good chance of being correct; $2.7 < Z < 2.9$, borderline significant, possibly correct; $2.0 < Z < 2.7$, poor score, could be right, but needs other confirmation."

Rank	*Z*-score	Code	Name
1	3.37	1lfa	αL I domain
2	3.13	1jlm	αM I domain
3	2.76	1chd	Cheb methylesterase[a]
4	2.56	1zon	αL I domain
5	2.48	1ido	αM I domain
6	2.41	1auq	VWF A1 domain
7	2.39	1ao3	VWF A3 domain

[a] Catalytic domain of the *Salmonella* chemotaxis receptor methylesterase, Cheb, which has a Rossmann fold.

known as the Rossmann, or nucleotide-binding, fold and has some features that may be significant for the β subunit I-like domain that will be discussed below. The *Z*-scores for I domains and 1chd are in a moderately high range that suggests that the I-like domain has a Rossmann fold and has structurally significant similarities to integrin I domains. Since the scores are only moderately high and a domain with a different type of Rossmann fold is also present in the high scoring group, significant differences with I domains are also likely to exist. This justifies the "I-like" designation, to emphasize both similarities and differences with I domains.

Consistent with the threading results, sequence alignment with I domains reveals significant similarities and differences (Fig. 4). Integrin I domains and vWF A domains, referred to generically as I domains, were structurally superimposed to yield a structure-sequence alignment, and the β2 I-like domain was then aligned using both sequence and secondary structure similarities. The beginning of the β-subunit I-like domain can easily be aligned with I domains, using sequence similarities in the β1-strand, the D*X*S*X*S motif of the MIDAS, and hydrophobic residues in the α1-helix (Fig. 4). The predicted β2-strand of the I-like domain can also be aligned with the β2-strand of the I domain by sequence. The last 60 residues of the I and I-like domains can be equivalenced based on their alternating α4, β5, α5, β6, and α6 secondary structure units and because the α6-helix is the last predicted α-helix in the entire β subunit (Fig. 3). Sequences in this region can be aligned based on secondary structure prediction and hydrophobic amino acids (Fig. 4).

In Rossmann folds, the central β-strands are the longest and most hydrophobic. In I domains, β-strands 4 and 1 are central. The β4-strand of the I-like domain is readily identified by its hydrophobicity and sequence similarity to the β4-strand of I domains (Fig. 4). Alignment of the region with the β3-strand and α2- and α3-helices is difficult, but it is aided by the position of the neighboring β4-strand. Because alignment of β3, α2, and α3 is difficult and there is a weakly predicted β-strand in the I-like domain between the α2 and α3 helices, it is possible that the I and I-like domains could differ in topology in this region. The alignment in Fig. 4 indicates regions predicted to be correctly aligned (*white bars*), aligned with the correct secondary structural unit but perhaps offset in sequence (*light gray bars*) and of uncertain topology (*dark gray bar*). The alignment is similar to that of Ref. 19 and very different from that of Ref. 18.

Two long insertions in the I-like domain account for its greater length compared with I domains. A long loop in I-like domains, the specificity-determining loop, is inserted between β-strands 2 and 3, and a long sequence with two weakly predicted β-strands is inserted between β4 and α4 (Fig. 4).

In I domains, the order of β-strands is 6-5-4-1-2-3 (the same numbering is used for the I-like domain model; Fig. 5*A*). The C termini of β-strands 6, 5, 4, 1, and 2 are at the "top," as is the MIDAS. The α-helices α6, α1, and α2 form the "front" face, and α-helices α3, α4, and α5 form the "back" face, with a counterclockwise order viewed from the top of 1-2-3-4-5-6 surrounding the hydrophobic β-sheet (see I-like domain model; Fig. 5*A*).

The major differences between the I and I-like domains (*i.e.* the regions of uncertain topology and the two long insertions) are localized to its "right" and "back" sides (*gray main chain trace* in Fig. 5, *A* and *B*). The β3-strand and α2-helix of uncertain alignment topology are located in this region, as are the long insertions between the β2- and β3-strands and between the β4 and α4 elements. Notably, I domains differ from their close structural homologues, the small Ras-like G proteins, in this same region on the right side of the domain; furthermore, the differences between I domains and 1chd, the other top hit in threading, occur in this region. The α3-helix in the I-like domain is more hydrophobic than other I-like domain α-helices (Fig. 4) and resembles a hydrophobic α-helix in the same structural location in 1chd, which neighbors and is partly buried by two "extra" β-strands. The long insertion between β4 and α4 in the I-like domain probably has a similar structural location (but not topology) to the extra β-strands in 1chd, because this loop is disulfide-bonded to the α3-helix. Appropriately, the long loop buries the hydrophobic α3-helix in the I-like domain model (Fig. 5*A*). Nearby, the specificity-determining loop (57) between β-strands 2 and 3 is predicted to project from the top of the I-like domain.

The molecular model of the β2 subunit I-like domain (Fig. 5,

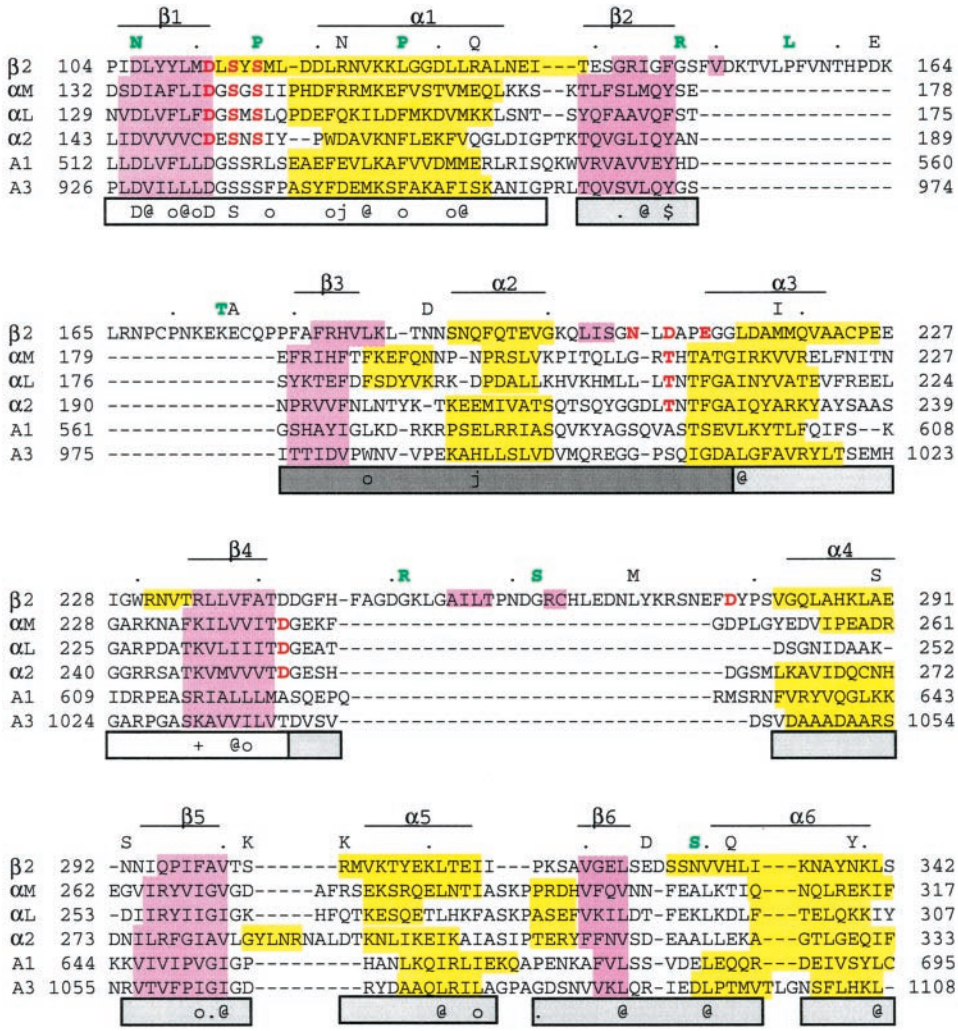

FIG. 4. **Alignment of the human β2 I-like domain with integrin I domains and vWF A domains.** Five I and A domain high resolution structures were structurally superimposed as described under "Materials and Methods" to yield the shown structure-sequence alignment. The β2 I-like domain was then aligned according to its sequence and predicted secondary structure. β-Strand and α-helix segments are highlighted in *pink* and *yellow*, respectively, as predicted for the human β2 I-like domain with PHD (49) using a multiple alignment of 35 β subunit sequences or determined for structures of I and A domains with DSSP (76). Above the human β2 sequence are shown residues that differ in mouse (*black*) or that are mutated in LAD (*green*) (14, 68). *Dots above* the human β2 sequence show every 10th residue. Residues in the primary or secondary coordination shell of the I domain structures are *red*. Conserved residues with oxygenated side chains in β2 are colored *red* if mutations of a particular residue in all tested β subunits (β1, β2, β3, and β5) abolished ligand binding and not subunit expression (18, 62, 71, 77, 78). The confidence in the alignment between the β-subunit and I domains is coded in the *bottom bar* as follows: correct (*white bar*); aligned with correct secondary structural unit but perhaps offset in sequence (*light gray*); uncertain topology (*dark gray*). Consensus sequences are as follows: aliphatic hydrophobic (@); hydrophobic (*o*); charged (*j*); small (*dot*); aromatic hydrophobic ($); positively charged (+).

A and *B*) was constructed with LOOK and MODELLER, as described under "Materials and Methods." All five I domains were used as templates, using the alignment shown in Fig. 4. Frameworks were provided for modeling portions of the two long insertions, but the only restraint on orientation relative to the rest of the I-like domain was the disulfide bond between Cys^{224} and Cys^{264}. The quality of the models was evaluated with programs developed to check the quality of x-ray and NMR structures and models, using structural features that differ from those used in refinement (58, 64) (Table IV). The quality of the β2 model is in a range that suggests that it is correctly threaded. The quality is better than for a previously described β3 model with a markedly different alignment and C-terminal domain boundary. Furthermore, the β2 model includes two long untemplated loops, which cannot be accurately modeled and decrease model quality. When these loops are deleted to give a model with the same number of residues as in the β3 model, the quality is markedly better than for the previous model (Table IV).

DISCUSSION

Our studies with mAb to the β2 integrin subunit provide a structure-function map and support a specific structure-sequence alignment and model for the I-like domain. The 12 mAb we mapped to the I-like domain recognized five sets of different epitopes, yet all inhibited binding of LFA-1 to ICAM-1 and ICAM-3 as measured in homotypic adhesion assays. This confirms the importance in β2 function of this domain, as previously suggested by its evolutionary conservation, the high incidence of mutations in this domain in LAD, and mutation of MIDAS residues. Of three mAb that mapped to a region between the C terminus of the I-like domain and the midpoint of the cysteine-rich region, none inhibited LFA-1 function. By contrast, two activating antibodies (28, 29), CBR LFA-1/2 and KIM185, mapped to the C-terminal half of the cysteine-rich domain (Fig. 3).

The epitopes of several β1, β2, and β3 activation antibodies have been mapped to regions close to residues 522–612, to

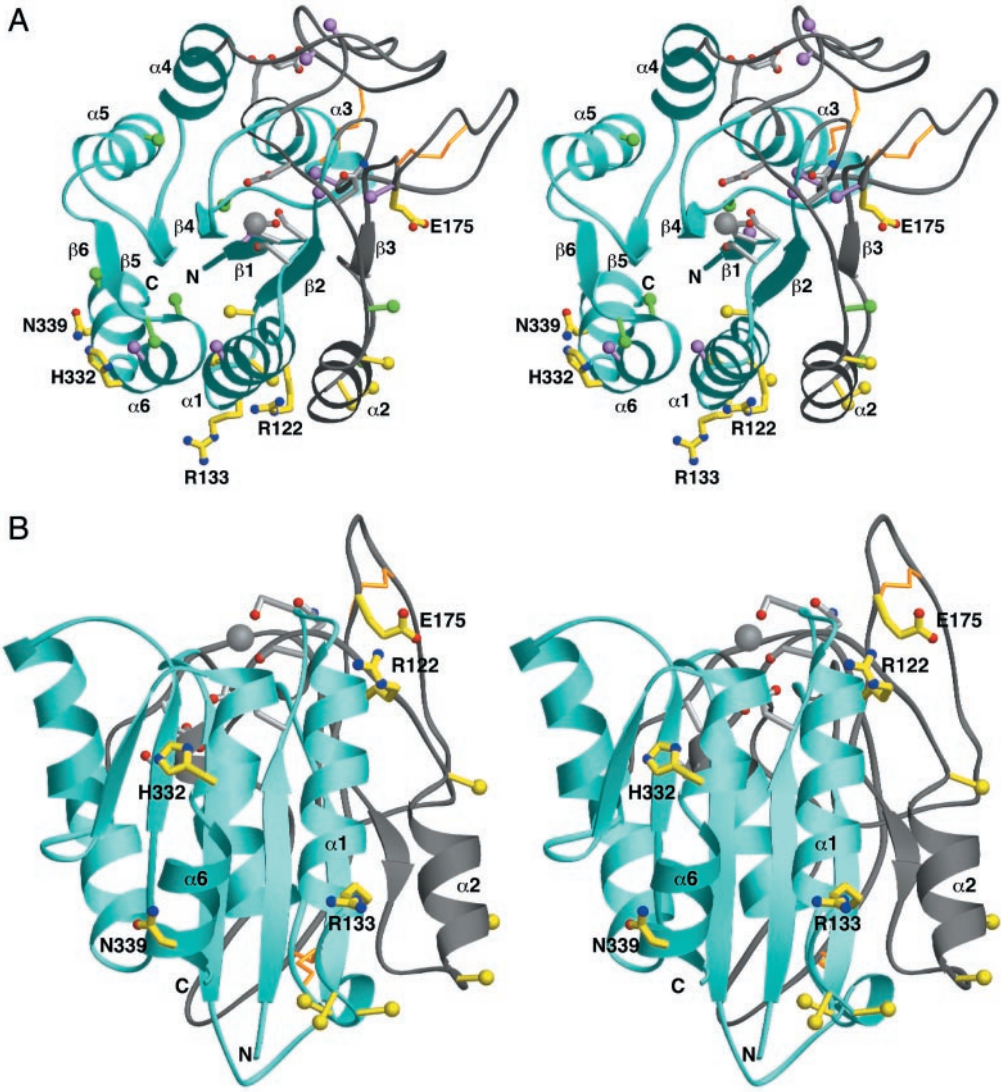

FIG. 5. **Stereodiagram of the β2 I-like domain model.** *A*, view of the top of the domain centered on the Mg^{2+} ion. *B*, view of the front of the domain centered on α-helices α1 and α6. *B*, rotated about an axis through the center of each β-strand 90° relative to *A*. The *ribbon diagram* (79) backbone is in *blue and gray* for areas of confident and uncertain topology, respectively. Oxygen and nitrogen atoms are *red* and *blue*, respectively. Antigenic residues in human β2 have *yellow* side chains. Positions corresponding to antigenic residues in human β1 (17) and chicken β1 (80) are shown as *yellow lollipops* with Cα–Cβ bonds and large Cβ atoms. Residues with oxygen-containing side chains important in ligand binding (see Fig. 4) have *silver* side chains. Mg^{2+} is represented as a *large silver sphere*. The two disulfide bonds are shown in *yellow*. In *A*, mutations in LAD and *N*-linked sites are shown. Residues mutated in LAD, except those with oxygen-containing side chains shown with *silver* side chains, are represented with *purple lollipops*. Positions corresponding to *N*-linked sites in at least 2 of 35 β-subunits appear as *green lollipops*. Note that antigenic residues and *N*-linked residues are exposed, while residues mutated in LAD are often buried. Note the absence of antigenic residues and *N*-linked sites on the α3- and α4-helices and the long loops on the "right" and "back" sides of the domain.

which CBR LFA-1/2 and KIM185 map. mAb KIM185 has independently been mapped to an overlapping region of residues 406–570 (27). Similarly, KIM127, another β2 activation antibody, has been mapped to the region of residues 406–570 (27). LIBS2, which can increase the affinity of the platelet integrin αIIbβ3 to fibrinogen by 20-fold, was localized within an 89-amino acid residue region immediately next to the transmembrane domain (21). TASC, an β1 integrin-activating antibody that promotes adhesion to laminin, binds to the region from residue 493 to 602 (16). Since the large number of disulfides in the C-terminal half of the cysteine-rich region should keep it rigid, it is hard to imagine that antibodies that bind to this region could induce a conformational change in the β subunit that would be propagated to the N-terminal region where the ligand binding sites are located. On the other hand, it seems likely that antibodies binding to this region could act like a "wedge" to keep the region to which they bind in the β subunit further apart from the α subunit and thus alter the relative orientation of the α and β subunits in the more N-terminal ligand binding region. The epitope of a mAb "G" to β1 (16) that has been shown to disrupt αβ subunit association was mapped to the same region. Therefore, this region may have an important function in transducing inside-out signals from the cytoplasm to the ligand-binding head piece of integrins.

Although it has been proposed that the evolutionarily conserved region of integrin β subunits contains a MIDAS and adopts an I domain fold (8), this proposal has been clouded by disagreement on the C-terminal boundary of the domain (18, 19), a lack of consistent threading predictions, and lack of any experimental evidence in support of a particular topology. Our alignment is similar overall in the secondary structure elements that are equivalenced to that of Tuckwell and Humphries (19), although different in many alignment positions, and differs dramatically from that of Tozer *et al.* (18). We provide computational and experimental evidence for a particular structure-sequence alignment and qualify the confidence

TABLE IV
Model evaluation

Model	Residues	QUACHK score[a]	NQACHK score[b]
β2[c]	239	−1.265	−3.80
β3[d]	181	−1.465	−4.00
β2 with loops deleted[e]	181	−0.998	−3.44

[a] Structural average packing environment quality score with the quality check (QUACHK) option of WHATIF. Higher (less negative) values are better. Scores receive the following messages: <-2.7, error, certain to be wrong; -2.7 to -2.0, error, quality is very low; -2.0 to -1.4, warning, quality is a bit low; > -1.4, note, quality is within normal ranges.

[b] New or second generation average structural packing environment *Z*-score with the NQACHK option of WHATIF. Higher (less negative) values are better. The average *Z*-score for properly refined x-ray structures is 0.0 ± 1.0. Scores receive the following messages: < -5.0, error, the structure is certain to be incorrect; -5.0 to -4.0, error, abnormal score, quality is very low; -4.0 to -3.0, warning, quality is a bit low, the protein is probably threaded correctly; > -3.0, note, quality is within normal ranges.

[c] β2 I-like domain model described here.

[d] β3 I-like domain model previously described by Tozer *et al.* (18).

[e] β2 I-like domain with untemplated loops from residues 150–177 and 248–277 deleted, to give the same number of residues as in the Tozer *et al.* model (18).

in different parts of this alignment. Secondary structure predictions on the entire β2 extracellular domain defined a specific segment with alternating α-helices and β-strands. This alternating pattern is characteristic of α/β folds, and we identified it with the I-like domain. Threading predictions on this segment averaged from 35 different integrin β subunits consistently identified I domains and another domain with a Rossmann fold as the top hits. The beginning and end of the I-like domain could be clearly aligned with the I domain, as could the central β4-strand. Model building provided support for the structure-sequence alignment, because the structural quality was better than for a model derived with a different alignment. Finally, mAb mapping showed that residues 133, 332, and 339 are adjacent in the three-dimensional structure. This evidence is independent of, and hence reinforces, the secondary structure prediction and sequence alignment that suggest these residues are in adjacent α-helices. The fold is clearly similar overall to that of I domains but also different in some respects. We explicitly acknowledge uncertainty in the threading of β3 and α2 and two inserted loops that are untemplated by different *color codes* in Figs. 4 and 5. Furthermore, we cannot rule out a contribution by β-strands N-terminal to residue 104 or C-terminal to residue 342 to the I-like domain.

Mapping with six different mAbs, which recognize three distinct epitopes, demonstrate that residues 133, 332, and 339 are adjacent in the structure. Each pair of these residues is recognized by a different group of antibodies. The proximity of these residues confirms our structure-sequence alignment and three-dimensional model, which places these residues in structurally adjacent α-helices 1 and 6. Residues 332 and 339 are exactly two helix turns apart in predicted α-helix 6, as appropriate for presence on the same face of this helix. In the model, residues 133, 332, and 339 form an almost equilateral triangle, with their Cα carbons 12.8–14.9 Å distant (Fig. 5*B*). Each pair of residues can readily be encompassed in an antibody footprint, which is approximately 30 Å in diameter.

Of overall interest for integrin domain organization, we can predict which faces of the I-like domain are solvent-exposed and, conversely, which are not exposed and thus may interact with other domains in the integrin α and β subunits. The predicted helices α1 and α6 are highly exposed in the intact integrin, as shown by antibody recognition of residues Arg^{122}, Arg^{133}, His^{332}, and Asn^{339} (Fig. 5, *A* and *B*). Residues recognized by inhibitory mouse mAb to chicken β1 map nearby to the end of the α1-helix and the loop connecting it to the β2-strand (*yellow lollipops* in Fig. 5, *A* and *B*). Activating and inhibitory mAb to human β1 map to the neighboring α2-helix (*yellow lollipops* in Fig. 5, *A* and *B*). Therefore, the "front" face of the I-like domain that bears the α6, α1, and α2 helices is well exposed in the intact integrin, and this includes residues that extend from the top of this face to the bottom of the domain. The location of the antigenic residue Glu^{175} is much less certain, but it appears to be not far from the other antigenic residues, near the "top right" of the domain. *N*-Linked glycosylation sites also define surface-exposed sites (*green lollipops* in Fig. 5*A*). They map to the front and bottom of the domain, and to the top left side on α helices 5 and 6. The "back" of the domain including much of α5, α4, α3, and the long inserted loops on the back and right of the domain, are therefore free for interactions with other integrin domains. The long insertion between β4 and α4 that is disulfide-bonded to α3 is in this region. The long insertion between β2 and β3 is nearby. It is interesting that the long insertions in the I-like domain relative to the I domain occur on the less accessible faces and may represent specializations for interactions with other domains.

Since both the β-subunit I-like domain and α-subunit β-propeller domain contribute to integrin specificity for ligands, they may associate with one another in the ligand binding integrin head piece. Extensive interactions between the I-like domain and other integrin domains are in keeping with our inability to express isolated, folded β2 or β1 I-like domains[2] and with studies on the requirement for αβ subunit association for antibody reactivity with the β2 subunit I-like domain (65). Nine of the 10 mAbs to the I-like domain studied here are completely dependent on association of β2 with a leukocyte integrin α subunit for reactivity. By contrast, mAb to the segments N- and C-terminal to the I-like domain react equally well with the β2 subunit whether it is free or complexed with α. The 1C11 mAb to the I-like domain is intermediate; it reacts with isolated β, although less well than with αβ complex. This mAb recognizes Arg^{133} and Asn^{339} at the bottom of the front face of the I-like domain (Fig. 5*B*); the base of the I-like domain may be stabilized by connections at the base of the domain to the N- and C-terminal β-subunit segments that fold independently of α (Fig. 3). Reciprocally to the requirement for folding of the I-like domain on α subunit association, folding of the β-propeller domain in the α subunit is dependent on β subunit association (66, 67). Therefore, it is attractive to speculate that the α-subunit β-propeller domain may associate directly with the β subunit I-like domain through one of the sites we have identified here, on the back, right, or upper faces.

The residues that are mutated in LAD patients (14, 68) are shown as *pink lollipops* or *spheres* in Fig. 5*A* and *above* the β2 sequence in *green* in Fig. 4. These mutations prevent association of the α and β subunits and expression on the cell surface. The residues Asp^{106}, Leu^{127}, Gly^{147}, and Pro^{156} are predicted to be buried inside the molecule. Mutation of these residues is predicted to disrupt the packing of the I-like domain. Residues Gly^{251} and Gly^{262} are on the "back" of the I-like domain and may be in an interface with another domain. Asn^{329} and Lys^{174} are predicted to be exposed to solvent. The patient with the mutation of Asn^{329} has moderate deficiency, with expression of mutated β2 integrins at about 22% of the level of wild-type β2 integrins (69). Lys^{174} was reported to be mutated to Thr in LAD (70); however, we found that mutation of Lys^{174} to alanine does not affect expression on COS cells or binding of transfectants to ICAM-1 (not shown). Furthermore, this residue is Ser in the chicken β2 integrin subunit (14) and may represent a polymor-

[2] C. Huang, Q. Zang, J. Takagi, and T. A. Springer, unpublished data.

phic substitution rather than a substitution responsible for LAD.

Finally, the model is consistent with one or more metal binding sites on the top of the I-like domain. Residues that have oxygen-containing side chains that are conserved across β integrins are candidates for ligating metals and have been mutated in β1, β2, β3, and β5 integrins (15, 18, 62, 71, 72) Oxygenated residues that have been consistently found to be important for ligand binding all map to the top of the I-like domain (*red residues* in Fig. 4; *silver side chains* in Fig. 5, *A* and *B*). Three of these correspond to the D*X*S*X*S motif of the I domain MIDAS. In the loop between α2 and α3 where I domains have a ligating threonine, I-like domains have three implicated residues in an amino acid sequence of markedly different character (Fig. 4). An aspartic acid residue immediately following β-strand 4 is important in I domains but not in I-like domains; however, an important aspartic acid is found after the long insertion between β4 and α4 in I-like domains that may be in a similar position in the structure (Fig. 4). The presence of a MIDAS-like metal ion binding site at the top of the I-like domain is supported by the position in the model of the oxygenated residues that are important in ligand binding (Fig. 5, *A* and *B*), in agreement with conclusions of Puzon-McLaughlin and Takada (62). In I domains, alternative coordination geometries at the MIDAS regulate ligand binding and are linked to changes in tertiary structure (9, 73). Given the proximity of the MIDAS-like site in the I-like domain to potential interfaces with other integrin domains, it is tempting to speculate that alternative coordination geometries could regulate tertiary structure of neighboring domains and hence could indirectly regulate ligand binding to other domains as well as directly regulate binding to the I-like domain.

Acknowledgments—We thank Lorence H. Kim for technical assistance.

REFERENCES

1. Hynes, R. O. (1992) *Cell* **69,** 11–25
2. Springer, T. A. (1995) *Annu. Rev. Physiol.* **57,** 827–872
3. Springer, T. A. (1990) *Nature* **346,** 425–433
4. Anderson, D. C., and Springer, T. A. (1987) *Annu. Rev. Med.* **38,** 175–194
5. Diamond, M. S., and Springer, T. A. (1994) *Curr. Biol.* **4,** 506–517
6. Schwartz, M. A., Schaller, M. D., and Ginsberg, M. H. (1995) *Annu. Rev. Cell Dev. Biol.* **11,** 549–599
7. Springer, T. A. (1997) *Proc. Natl. Acad. Sci. U. S. A.* **94,** 65–72
8. Lee, J.-O., Rieu, P., Arnaout, M. A., and Liddington, R. (1995) *Cell* **80,** 631–638
9. Lee, J.-O., Bankston, L. A., Arnaout, M. A., and Liddington, R. C. (1995) *Structure* **3,** 1333–1340
10. Qu, A., and Leahy, D. J. (1995) *Proc. Natl. Acad. Sci. U. S. A.* **92,** 10277–10281
11. Emsley, J., King, S. L., Bergelson, J. M., and Liddington, R. C. (1997) *J. Biol. Chem.* **272,** 28512–28517
12. Staunton, D. E., Dustin, M. L., Erickson, H. P., and Springer, T. A. (1990) *Cell* **61,** 243–254
13. Huang, C., and Springer, T. A. (1995) *J. Biol. Chem.* **270,** 19008–19016
14. Bilsland, C. A. G., and Springer, T. A. (1994) *J. Leukocyte Biol.* **55,** 501–506
15. Loftus, J. C., Smith, J. W., and Ginsberg, M. H. (1994) *J. Biol. Chem.* **269,** 25235–25238
16. Shih, D. T. (1993) *J. Cell Biol.* **122,** 1361–1371
17. Takada, Y., and Puzon, W. (1993) *J. Biol. Chem.* **268,** 17597–17601
18. Tozer, E. C., Liddington, R. C., Sutcliffe, M. J., Smeeton, A. H., and Loftus, J. C. (1996) *J. Biol. Chem.* **271,** 21978–21984
19. Tuckwell, D. S., and Humphries, M. J. (1997) *FEBS Lett.* **400,** 297–303
20. Bork, P., Doerks, T., Springer, T. A., and Snel, B. (1999) *Trends Biochem. Sci.* **24,** 261–263
21. Du, X., Gu, M., Weisel, J. W., Nagaswami, C., Bennett, J. S., Bowditch, R., and Ginsberg, M. H. (1993) *J. Biol. Chem.* **268,** 23087–23092
22. Bazzoni, G., Shih, D.-T., Buck, C. A., and Hemler, M. A. (1995) *J. Biol. Chem.* **270,** 25570–25577
23. Yednock, T. A., Cannon, C., Vandevert, C., Goldbach, E. G., Shaw, G., Ellis, D. K., Liaw, C., Fritz, L. C., and Tanner, L. I. (1995) *J. Biol. Chem.* **270,** 28740–28750
24. Puzon-McLaughlin, W., Yednock, T. A., and Takada, Y. (1996) *J. Biol. Chem.* **271,** 16580–16585
25. Luque, A., Gomez, M., Puzon, W., Takada, Y., Sanchez-Madrid, F., and Cabanas, C. (1996) *J. Biol. Chem.* **271,** 11067–11075
26. Takagi, J., Isobe, T., Takada, Y., and Saito, Y. (1997) *J. Biochem.* (*Tokyo*) **121,** 914–921
27. Stephens, P., Romer, J. T., Spitali, M., Shock, A., Ortlepp, S., Figdor, C., and Robinson, M. K. (1995) *Cell Adhes. Commun.* **3,** 375–384
28. Petruzzelli, L., Maduzia, L., and Springer, T. (1995) *J. Immunol.* **155,** 854–866
29. Andrew, D., Shock, A., Ball, E., Ortlepp, S., Bell, J., and Robinson, M. (1993) *Eur. J. Immunol.* **23,** 2217–2222
30. Sanchez-Madrid, F., Krensky, A. M., Ware, C. F., Robbins, E., Strominger, J. L., Burakoff, S. J., and Springer, T. A. (1982) *Proc. Natl. Acad. Sci. U. S. A.* **79,** 7489–7493
31. David, V., Leca, G., Corvaia, N., Le Deist, F., Boumsell, L., and Bensussan, A. (1991) *Cell Immunol.* **136,** 519–524
32. Miedema, F., Tetteroo, P. A. T., Hesselink, W. G., Werner, G., Spits, H., and Melief, C. J. M. (1984) *Eur. J. Immunol.* **14,** 518–523
33. Hildreth, J. E. K., Gotch, F. M., Hildreth, P. D. K., and McMichael, A. J. (1983) *Eur. J. Immunol.* **13,** 202–208
34. Keizer, G. D., Borst, J., Figdor, C. G., Spits, H., Miedema, F., Terhorst, C., and de Vries, J. E. (1985) *Eur. J. Immunol.* **15,** 1142–1147
35. Pedrinaci, S., Huelin, C., Patarroyo, M., Ruiz-Cabello, F., and Garrido, F. (1989) *Hybridoma* **8,** 13–23
36. Bazil, V., Stefanova, I., Hilgert, I., Kristofova, H., Vanek, S., and Horejsí, V. (1990) *Folia Biol.* (*Prague*) **36,** 41–50
37. Ohashi, Y., Tsuchiya, S., Fujie, H., Minegishi, M., and Konno, T. (1992) *J. Exp. Med.* **167,** 297–299
38. Pope, I., Hale, G., and Waldmann, H. (1989) in *Leukocyte Typing IV* (Knapp, W., Dorken, B., Gilks, W. R., Rieber, E. P., Schmidt, R. E., Stein, H., and von dem Borne, A. E. G. K., eds) 4th Ed., pp. 559–560, Oxford University Press, Oxford
39. Knapp, W., Dörken, B., Gilks, W. R., Rieber, E. P., Schmidt, R. E., Stein, H., and von dem Borne, A. E. G. K. (1989) *Leucocyte Typing IV: White Cell Differentiation Antigens*, Oxford University Press, Oxford
40. Schlossman, S. F., Boumsell, L., Gilks, W., Harlan, J., Kishimoto, T., Morimoto, T., Ritz, J., Shaw, S., Silverstein, R., Springer, T., Tedder, T., and Todd, R. (eds) (1995) *Leukocyte typing V: White Cell Differentiation Antigens*, Oxford University Press, Oxford
41. Trowbridge, I. S., and Omary, M. B. (1981) *J. Exp. Med.* **154,** 1517–1524
42. Kishimoto, T. K., O'Connor, K., Lee, A., Roberts, T. M., and Springer, T. A. (1987) *Cell* **48,** 681–690
43. Ho, S. N., Hunt, H. D., Horton, R. M., Pullen, J. K., and Pease, L. R. (1989) *Gene* (*Amst.*) **77,** 51–59
44. Aruffo, A., and Seed, B. (1987) *Proc. Natl. Acad. Sci. U. S. A.* **84,** 8573–8577
45. DuBridge, R. B., Tang, P., Hsia, H. C., Leong, P. M., Miller, J. H., and Calos, M. P. (1987) *Mol. Cell. Biol.* **7,** 379–387
46. Heinzel, S. S., Krysan, P. J., Calos, M. P., and DuBridge, R. B. (1988) *J. Virol.* **62,** 3738–3746
47. Hibbs, M. L., Wardlaw, A. J., Stacker, S. A., Anderson, D. C., Lee, A., Roberts, T. M., and Springer, T. A. (1990) *J. Clin. Invest.* **85,** 674–681
48. Gotoh, O. (1996) *J. Mol. Biol.* **264,** 823–838
49. Rost, B. (1996) *Methods Enzymol.* **266,** 525–539
50. Jones, D. T., Miller, R. T., and Thornton, J. M. (1995) *Proteins Struct. Funct. Genet.* **23,** 387–397
51. Springer, T. A. (1998) *J. Mol. Biol.* **283,** 837–862
52. Orengo, C. A., Michie, A. D., Jones, S., Jones, D. T., Swindells, M. B., and Thornton, J. M. (1997) *Structure* **5,** 1093–1108
53. Qu, A., and Leahy, D. J. (1996) *Structure* **4,** 931–942
54. Emsley, J., Cruz, M., Handin, R., and Liddington, R. (1998) *J. Biol. Chem.* **273,** 10396–10401
55. Huizinga, E. G., Martijn van der Plas, R., Kroon, J., and Sixma, J. J. (1997) *Structure* **5,** 1147–1156
56. Sali, A., and Blundell, T. L. (1993) *J. Mol. Biol.* **234,** 779–815
57. Takagi, J., Kamata, T., Meredith, J., Puzon-McLaughlin, W., and Takada, Y. (1997) *J. Biol. Chem.* **272,** 19794–19800
58. Vriend, G. (1990) *J. Mol. Graph.* **8,** 52–56
59. Larson, R. S., Hibbs, M. L., and Springer, T. A. (1990) *Cell Regul.* **1,** 359–367
60. de Fougerolles, A. R., Stacker, S. A., Schwarting, R., and Springer, T. A. (1991) *J. Exp. Med.* **174,** 253–267
61. de Fougerolles, A. R., and Springer, T. A. (1992) *J. Exp. Med.* **175,** 185–190
62. Puzon-McLaughlin, W., and Takada, Y. (1996) *J. Biol. Chem.* **271,** 20438–20443
63. Edwards, Y. J. K., and Perkins, S. J. (1996) *J. Mol. Biol.* **260,** 277–285
64. Wilson, K. S., Butterworth, S., Dauter, Z., Lamzin, V. S., Walsh, M., Wodak, S., Pontius, J., Richelle, J., Vaguine, A., Sander, C., Hooft, R. W. W., Vriend, G., Thornton, J. M., Laskowski, R. A., Macarthur, M. W., Dodson, E. J., Murshudov, G., Oldfield, T. J., Kaptein, R., and Rullmann, J. A. C. (1998) *J. Mol. Biol.* **276,** 417–436
65. Huang, C., Lu, C., and Springer, T. A. (1997) *Proc. Natl. Acad. Sci. U. S. A.* **94,** 3156–3161
66. Huang, C., and Springer, T. A. (1997) *Proc. Natl. Acad. Sci. U. S. A.* **94,** 3162–3167
67. Lu, C., Oxvig, C., and Springer, T. A. (1998) *J. Biol. Chem.* **273,** 15138–15147
68. Wright, A. H., Douglass, W. A., Taylor, G. M., Lau, Y.-L., Higgins, D., Davies, K. A., and Law, S. K. (1995) *Eur. J. Immunol.* **25,** 717–722
69. Nelson, C., Rabb, H., and Arnaout, M. A. (1992) *J. Biol. Chem.* **267,** 3351–3357
70. Arnaout, M. A., Dana, N., Gupta, S. K., Tenen, D. G., and Fathallah, D. M. (1990) *J. Clin. Invest.* **85,** 977–981
71. Bajt, M. L., and Loftus, J. C. (1994) *J. Biol. Chem.* **269,** 20913–20919
72. Bajt, M. L., Goodman, T., and McGuire, S. L. (1995) *J. Biol. Chem.* **270,** 94–98
73. Oxvig, C., Lu, C., and Springer, T. A. (1999) *Proc. Natl. Acad. Sci. U. S. A.* **96,** 2215–2220
74. Rothlein, R., Dustin, M. L., Marlin, S. D., and Springer, T. A. (1986) *J. Immunol.* **137,** 1270–1274
75. Calvete, J. J., Henschen, A., and González-Rodríguez, J. (1991) *Biochem. J.* **274,** 63–71
76. Kabsch, W., and Sander, C. (1983) *Biopolymers* **22,** 2577–2637
77. Lin, E. C. K., Ratnikov, B. I., Tsai, P. M., Gonzalez, E. R., McDonald, S., Pelletier, A. J., and Smith, J. W. (1997) *J. Biol. Chem.* **272,** 14236–14243
78. Goodman, T. G., and Bajt, M. L. (1996) *J. Biol. Chem.* **271,** 23729–23736
79. Carson, M. (1991) *J. Appl. Crystallogr.* **24,** 958–961
80. Shih, D. T., Doettiger, D., and Buck, C. A. (1997) *J. Cell Sci.* **110,** 2619–2628